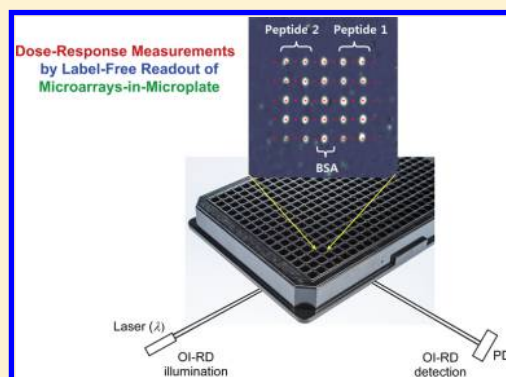


High-Throughput Dose–Response Measurement Using a Label-Free Microarray-in-Microplate Assay Platform

J. P. Landry, G. Malovichko, and X. D. Zhu*

Department of Physics, University of California at Davis, Davis, California 95616, United States

ABSTRACT: Microarray-based binding assays facilitate the discovery of protein ligands from large collections of small molecules. Hundreds of ligands can be identified, yet only a small portion of them have interfering effects (competitive or noncompetitive) on a specific protein–receptor binding reaction. Further efficient screening of ligands for those with specific modifying effect is needed in order to take the full advantage of throughputs of microarray-based assays for drug discovery. We report a *label-free* “microarray-in-microplate” assay platform for simultaneous acquisition of at least 32 dose–response curves in a single experiment, each curve having 12 concentration points. When combined with ligand discovery, this makes the microarray-based platform a true high-throughput means of finding inhibitors to specific protein–receptor reactions starting from a large collection of small-molecule libraries.



Networks of protein–ligand interactions collectively determine the function, health, and life-cycle of an organism. Characterization and alteration of these interactions and their networks drive molecular and cellular biology and enable drug discovery against diseases. For drug development based on small-molecule ligands (MW < 1000 Da), one needs to identify lead molecules that have desirable interfering effects on specific protein–receptor interactions.^{1–6} This usually involves screening thousands to millions of molecules for ligands of a target protein with suitable binding affinity. Most currently used biochemical assays for high-throughput screening are based on high-density microplates and on detection of light emission (fluorescence or luminescence) or reflection (surface plasmon resonance or waveguide-resonance or bilayer interferometry) from or color change in or mass spectra of reaction mixes. Depending upon target proteins or receptors some of these assays identify ligands from a large collection of small-molecule compounds and further reveal directly whether the ligands have desirable functional effects. Small-molecule microarrays are platforms that also serve for such needs.^{7–12} For example, Landry et al. demonstrated that over 50 000 small-molecule compounds can be screened in 2 days against a target based on binding curve measurements on small molecule microarrays.¹⁰ With several such assay systems operating in parallel on prefabricated small-molecule microarrays it is realistic to screen one million compounds for ligands of a target in less than 2 weeks.

Typically, a fraction of a percent to a few percent of the screened molecules show adequate affinity to a protein and are thus considered ligands of the protein. Although such a ligand collection is much smaller than the original compound collection, it is still relatively large, typically in the range of hundreds or more. This is because a bulky protein molecule presents many binding sites accessible to a wide variety of small

molecules. For drug discovery against a target protein in a signaling pathway one is only concerned with the binding site where a specific protein–receptor interaction takes place and thus only those ligands that modify the property of this particular site, directly or allosterically. To find these special ligands one needs to further screen the ligand collection using a suitable inhibition assay that measures dose–response curves of all ligands in the collection. Unlike screening library compounds for ligands of a protein in which reactions of the protein with tens of thousands (in label-free detection) or even millions (in fluorescence-based detection) of molecular candidates can be performed simultaneously on assay platforms such as microarrays^{7–9,11,13} or bead libraries,^{14–16} a dose–response measurement only involves the target protein, a receptor of interest, and one ligand at a time. One may reduce the number of full dose–response curves by initially running a single inhibition assay for each ligand at a suitably high concentration and only acquire dose–response curves for ligands that exhibit significant inhibition effect in the single-dose measurement. Microplate-based inhibition assays are ideal for high-throughput dose–response measurements, particularly if chemical luminescence or fluorescence methods are readily available to read out the assays. If label-free optical detection is desirable, waveguide-based sensors (e.g., Corning EPIC) or bilayer interference sensors (e.g., Fortebio Ortec) are commercially available.

In this report we describe a microarray-in-microplate assay platform that affords high-throughput dose–response measurement. This platform combines label-free detected microarrays^{10,17–19} with a microplate. By fabricating 384 small

Received: February 21, 2015

Accepted: April 28, 2015

Published: April 28, 2015

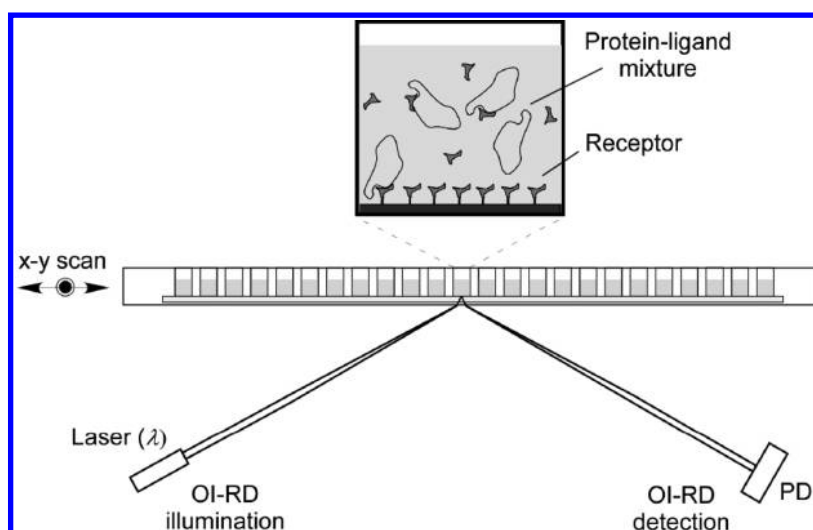


Figure 1. Label-free-detected microarrays in a microplate for high-throughput dose–response curve measurement. Microarrays of receptors are fabricated on a functionalized glass plate. The glass plate is bonded with a bottomless microplate to form a glass-bottomed microplate with printed receptor microarrays. Mixtures of a target protein at a fixed concentration and a ligand at 12 different concentrations are deposited in 12 wells, respectively, and incubate with the receptors simultaneously. A label-free optical sensor reads out surface densities of target–receptor complexes in real time. The equilibrium surface density as a function of ligand concentration forms a dose–response curve. A 384-well glass-bottomed microplate yields dose–response curves of 32 distinct ligands in a single experiment.

microarrays (each containing replicates of two distinct receptors) in wells of a glass-bottomed microplate, we demonstrate this platform by acquiring 64 dose–response curves in a single experiment, each curve having 12 ligand concentration points. Compared to waveguide-based sensors, this platform is more cost-effective, as microplates only need to have chemically functionalized glass plates instead of fabricated waveguide-structures at the bottom. Compared to bilayer interference sensors, the microarray-in-microplate platform generates from each well a set of readouts acquired under the same reaction condition in a single measurement and thus enables statistical analysis of the data without having to repeat the measurement on different plates.

MATERIALS AND METHODS

Figure 1 illustrates such microarray-in-microplate assay platform. Small microarrays of a receptor molecule are immobilized in 12 wells of a glass-bottomed microplate. Solutions of a ligand at 12 concentrations and a target protein at a fixed concentration are deposited in these wells, respectively. A label-free optical scanner records surface densities of protein–receptor complexes *during* incubation. Equilibrium surface densities of the complexes versus ligand concentration yield a dose–response curve against the protein–receptor binding. One 384-well plate enables simultaneous acquisition of dose–response curves of 32 distinct ligands against same or different protein–receptor reactions.

Fabrication of Microarrays in a 384-Well Functionalized Glass-Bottomed Microplate. We use microplates with optically flat and low-strain glass bottoms that support both microarray fabrication and subsequent optical detection. ProPlate 384 square well adhesive SBS microtiter plates without bottoms were purchased from Gracebio-Laboratories (Bend, OR). Epoxy-functionalized ProPlate glass, matching the microtiter plates, was purchased from ArrayIt (Sunnyvale, CA). By pressing a ProPlate glass to the adhesive bottom of a ProPlate 384 square well microtiter plate, we have a

functionalized glass-bottom microplate, ready for microarray fabrication.

For receptors, we use 64 synthetic peptides of 15 amino acids long (15-aa). They are derived from 64 proteins (see Table 1 for details). The peptides are terminated intentionally with cysteine residue for immobilization on epoxy-functionalized glass surface. Using an OmniGrid100 contact-printing robot (Digilab, Marlborough, MA), we print 10 replicates each of a pair of receptors and five replicates of bovine serum albumin (BSA) as controls in 12 wells. A total of 384 wells accommodate all 64 peptides. In a typical application one may print replicates of only one receptor in a well instead of two receptors.

For targets we use purified rabbit monoclonal antibodies, supplied by Epitomics, Inc. (Burlingame, CA) that are specifically raised against the 64 synthetic peptides. These are full-length antibodies and thus bivalent. Using a label-free optical scanner similar to the one used for this study, we separately measured equilibrium dissociation constants K_d of these rabbit monoclonal antibodies with the 64 peptides on functionalized glass slides. The values of K_d are listed in Table 1.

Label-Free Microplate Scanner for Detection of Microarrays in Microplate. One of the advantages of a scanning optical detection platform is the large expandable field of view (FOV).^{10,17–19} We built a special label-free optical scanner with a FOV of the size of a microplate ($\sim 60 \text{ cm}^2$) to read microarrays in a glass-bottomed microplate. It is based on measurements of oblique-incidence reflectivity difference (OI-RD) and will be called an OI-RD microplate reader.^{17,20,21} OI-RD is defined as $\Delta_p - \Delta_s \equiv (r_p - r_{p0})/r_{p0} - (r_s - r_{s0})/r_{s0}$, where r_{p0} and r_{s0} are reflectivities of a monochromatic light beam from a bare solid surface and r_p and r_s are the reflectivities from the solid surface when it is covered with the molecular layer. $\Delta_p - \Delta_s$ is proportional to the surface mass density Γ (g/cm^2) of the molecular layer.^{17,20,22} In our present dose–response curve measurement, $\Delta_p - \Delta_s$ is proportional to the surface mass density of protein–receptor complexes. Figure 2

Table 1. Original Proteins from Which 15-AA Peptides Are Derived; Affinity Constants (K_d) of Rabbit IgG (as Target Proteins) with Immobilized Peptides (as Receptors); IC50 of Peptides in Solution (as Inhibitory Ligands) against Complex Formation of IgG with Immobilized Receptors; Affinity Constants (K_i) of Ligands with Rabbit IgG^a

original proteins from which 15-aa peptides (receptors) are derived	affinity constant of target to immobilized receptor K_d (nM)	IC50 of inhibitory ligand (μ M)	standard error in IC50 (μ M)	affinity constant of target to inhibitory ligand K_i (nM)
CD34	0.12	2.8	0.4	3
paxillin	0.42	6	0.3	23
PCNA	0.77	23	4	176
calcitonin	0.21	6.4	0.5	13
HLA-DRA	0.17	9.1	1.3	15
cytokeratin 10 (CK10)	0.016	3.4	0.3	0.5
cytokeratin 17 (CK17)	0.25	2.0	0.2	5
myosin light chain 2 (MYL2)	0.28	0.41	0.04	0.9
p27-Kip1	0.021	11	3	2.2
TCL1	0.0051	5.0	0.5	0.25
SPP1	1.63	0.13	0.05	0.5
TNNT2	0.32	16	3	50
prostate-specific antigen (PSA)	0.50	30	3	148
ERG	0.89	1.1	0.1	9
OLIG2	0.015	0.24	0.01	0.02
cytokeratin 19 (R1579)	0.37	11.0	1.2	40
BOB-1	1.07	8		
Oct-2	0.47	8.0	0.8	37
fascin	1.4	3.1	0.4	43
HIF-1 α (HIF-1A)	0.22	0.54	0.07	1.0
survivin	0.44	4.8	0.4	21
c-Myc	0.0038	1.7	0.1	0.06
hemoglobin α chain (HBA1)	1.72	0.81	0.06	12
insulin	0.38	0.99	0.11	3.4
MMP-9	0.16	3.9	0.7	6
CD14	0.075	5.0	1.1	3.7
CD7	0.0024	1.1	0.1	0.023
aurora-B	0.055	2.4	0.5	1.2
PDX1	0.046	0.87	0.18	0.35
mesothelin	0.0055	0.41	0.04	0.017
glut-1	33000	0.05		
N-cadherin (CDH2)	530	0.8		
cytokeratin 4 (CK4)	0.58	2.1	0.3	12
CD99	9.40	1		
EGFR phospho (pY1068)	0.0	0.56	0.15	0.17
cytokeratin 15 (CK15)	0.56	0.66	0.05	3.1
cytokeratin 20 (CK20)	0.03	0.45	0.06	0.11
CDX2	0.010	69	9	7
progesterone receptor (PgR)	0.25	4.8	0.5	12
NGFR	3200	0.07		
S100 β (S100B)	4600	0.2		
chromogranin A (CgA)	0.0069	2.68	0.02	0.18
MART-1	1.27	2.1	0.3	25
CA 125	1100	0.9	0.5	0
ZAP-70	0.072	2.2	0.3	1.5
PMS2	0.15	2.3	0.8	3.2
CD44	0.38	1.5	0.3	5.3
CD90	0.16	3.1	0.3	4.6
cytokeratin 14 (CK14)	0.27	6.1	1.6	16
calponin-1	0.17	0.52	0.06	0.7
cytokeratin 6 (CK6)	0.42	0.8	0.2	2.8
CD45	0.04	6.6	1.2	2.4
cytokeratin 13 (CK13)	0.012	0.66	0.33	0.07
cytokeratin 19 (R1580)	4600	0.1		
glucagon	0.33	1.10	0.12	3.3
CD23	0.0055	5.9	0.8	0.32
CD5	0.017	0.4	0.1	0.044
CD1a	17.0	0.2		

Table 1. continued

original proteins from which 15-aa peptides (receptors) are derived	affinity constant of target to immobilized receptor K_d (nM)	IC50 of inhibitory ligand (μM)	standard error in IC50 (μM)	affinity constant of target to inhibitory ligand K_i (nM)
cathepsin D	0.12	4.4	0.6	5.0
CD79a-mb-1 (CD79a)	0.12	0.28	0.03	0.21
MCM5	0.15	0.21	0.02	0.17
MUC1	0.0089	0.47	0.03	0.033
L1-cadherin	0.0029	0.84	0.05	0.022
myoglobin	0.18	9.6	1.3	17

^aInitial concentration of rabbit IgG is 100 nM.

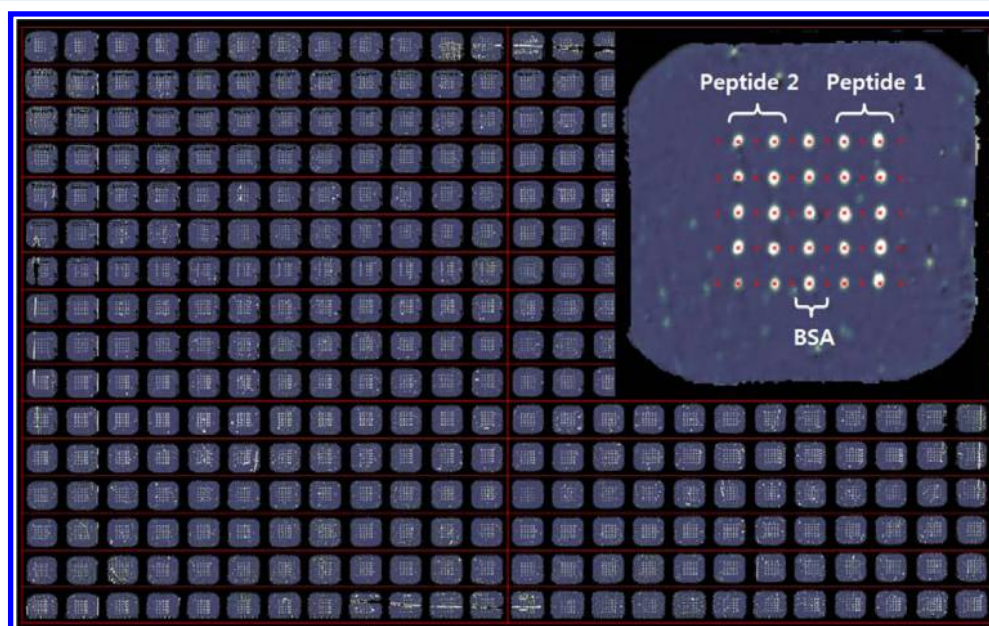


Figure 2. Oblique-incidence reflectivity difference (OI-RD) image of a glass-bottomed microplate printed with 384 receptor microarrays before incubation in target–ligand mixtures. Each receptor microarray has 25 spots (see inset): 10 replicates for each of two distinct receptors, and five replicates of bovine serum albumin (BSA) as a negative control. Crosses in the inset mark the pixels where optical signals are monitored in real time. The difference between the signal from the pixel inside a printed region (sample pixel) and the average of the two neighboring pixels (reference pixels) outside the printed region is used as the background-corrected signal and is proportional to the surface density of target–receptor complexes.

shows an OI-RD image of a glass-bottomed microplate with 384 peptide microarrays printed at the bottom. Thirty-two blocks of 12 wells are indicated in the image; each block is used to obtain dose–response curves for two peptide ligands at 12 concentrations. The inset shows details of a small microarray with 10 replicates for each of two peptide receptors and five replicates of BSA as control.

Dose–Response Curve Measurement. We deposit 30 μL of BSA at 1 mg/mL in 1 \times phosphate-buffered saline (PBS) in each well and incubate for 30 min to both remove excess receptors from the printed spots and block the unprinted surface so that the region between printed spots can be used as reference. We then acquire a baseline OI-RD image of the 384 receptor microarrays, similar to what is displayed in Figure 2.

We next add to 12 wells printed with same receptors 30 μL solutions of two ligands and the corresponding rabbit monoclonal antibodies (targets) in 1 \times PBS at concentrations such that after mixing with the preexisting BSA solution, each target has a fixed concentration of $[P]_0 = 100$ nM while the concentration of the two ligands varies from the first to the 12th well at 100 μM , 30 μM , 10 μM , 3 μM , 1 μM , 300 nM, 100 nM, 30 nM, 10 nM, 3 nM, 1 nM, and 0.3 nM, respectively. We let the microarrays incubate for 6 h so that the solutions reach equilibria with the immobilized receptors. Ligands in solution

form complexes with targets and in turn reduce the concentration of free targets ($[P]$). This process competes with the complex formation of targets with surface-bound receptors ($[R]$). IC50 (half-maximal inhibitory concentration) is the total ligand concentration $[I]_0$ at which the equilibrium surface density of the target–receptor complexes $[P\cdot R]$ is reduced by 50% from $[P\cdot R]_0$ obtained when $[I]_0 = 0$ (see the Appendix for details on how the equilibrium surface density of the complexes depends on various parameters).

To read out the surface density $[P\cdot R]$ of the target–receptor complexes in real time, we detect the OI-RD signal from the center of a printed target spot (sample pixel) and the signals from two positions in the neighboring unprinted region (reference pixels). The inset in Figure 2 shows an example of where sample pixels and reference pixels are selected. The difference between the signal from the sample pixel and the mean of the signals from the reference pixels is used as the final signal. It is proportional to the surface mass density of the target–receptor complexes. With 25 targets in each well and 384 wells altogether, it takes 5 min to perform one read-out for all 9600 targets as one time point. The optical measurement starts with a 30 min baseline (6 time points); after solutions of targets and ligands are added, the measurement proceeds further for 6 h (72 time points). We use the mean of the last 10

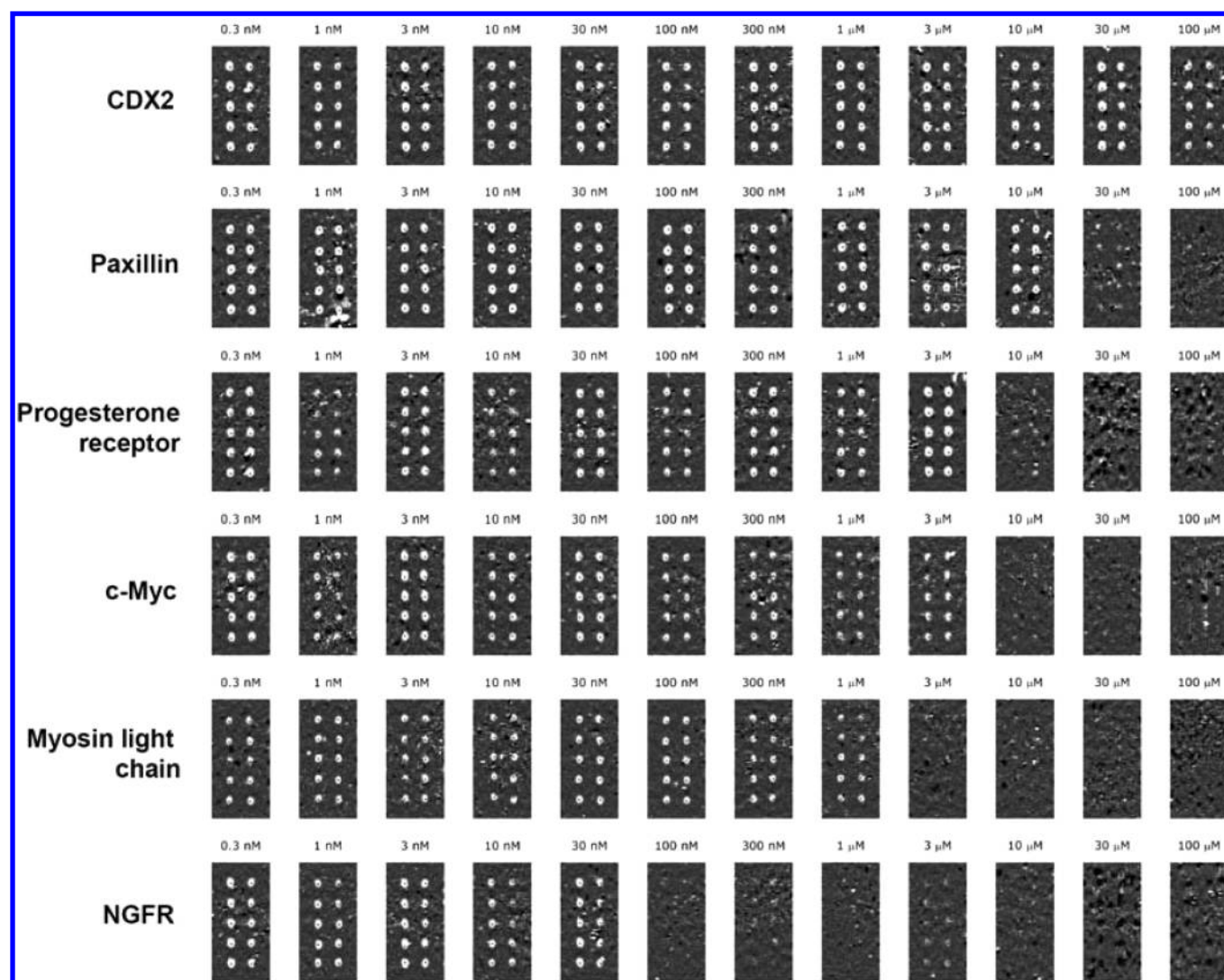


Figure 3. Differential OI-RD image of subarrays for six receptors as a function of ligand concentration, acquired by subtracting the image of the microplate taken before incubation from the image taken after the microarrays have been incubated in target–ligand mixtures for 6 h. The ligands in the solution in a well are the same as the immobilized receptors. The optical signals are proportional to surface densities of target–receptor complexes at equilibria.

time points as the signal corresponding to the equilibrium surface density of the target–receptor complexes. We further average the signals from 10 replicates in the well and compute both the mean and the standard error as the final data for each ligand concentration.

After the “real-time” dose–response measurement, we take another OI-RD image of the 384 microarrays and subtract from it the baseline image to obtain a differential image that reveals equilibrium surface mass densities of target–receptor complexes as a function of ligand concentration.

RESULTS AND DISCUSSION

Dose–Response Curves of 64 Ligands against the Complex Formation of Rabbit Monoclonal Antibodies with Immobilized Receptors. Figure 3 shows the differential OI-RD image, revealing equilibrium surface densities of target–receptor complexes as a function of ligand concentration, for six receptors. They are derived from CDX2, paxillin, progesterone receptor, c-Myc, myosin light chain, and NGFR (see Table 1). We can clearly see variations in the equilibrium surface density of the complexes as a function of ligand concentration. For

dose–response curves, we normalize the optical signals obtained at equilibrium (end of incubation) to the signals obtained in the absence of ligands. Figure 4 shows the normalized signals as a function of ligand concentration $[I]_0$ for all 64 ligands. The concentrations at which the signals reach 0.5 are readily identified. We define these concentrations (listed in Table 1) as *IC₅₀ for microarray-based dose–response assays* and explore next how these *IC₅₀* values are related to key parameters of the assays including affinity constants of target–receptor and target–inhibitor reactions.

Analysis of Dose–Response Curves and the Meaning of *IC₅₀* Values. In the present study, ligands (solution-phase peptides) inhibit the reaction of targets (rabbit monoclonal antibodies) with immobilized receptors (surface-bound peptides) by binding to same pockets on the targets. *IC₅₀* is the total ligand concentration at which the equilibrium concentration of target–receptor complexes is reduced by one-half from the level attained in the absence of the ligands. Applications of the Cheng–Prusoff equation for *IC₅₀*, derived in the same spirit as the Michaelis–Menten equation, require concentrations of both receptor and ligand to be much larger

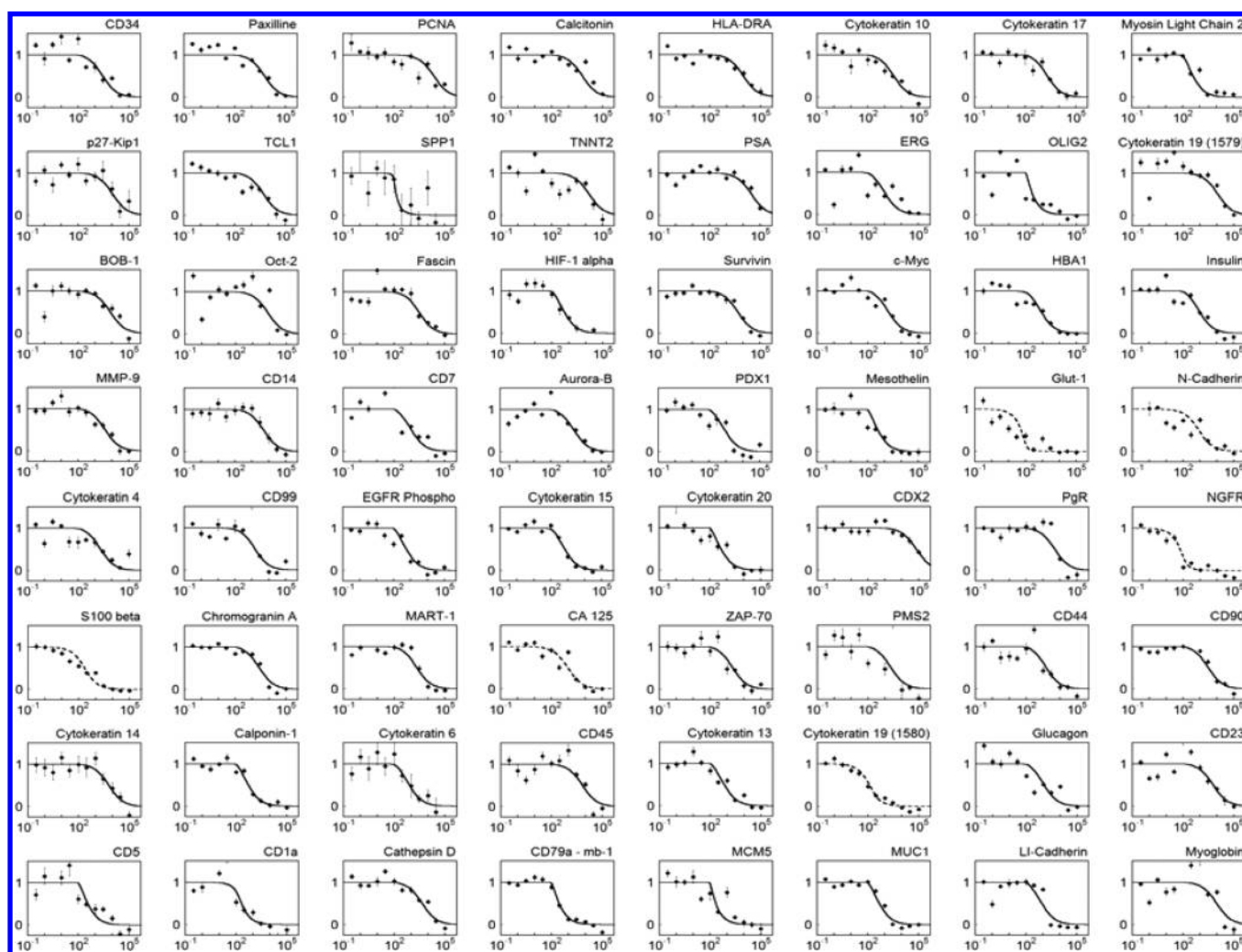


Figure 4. Sixty-four dose–response curves acquired from 384 receptor microarrays in a microplate. Each curve has 12 concentration points. Each point is the mean of the optical signals from 10 replicates divided by the mean of the signals obtained at concentrations far below the target concentration. The errors in the mean are also shown and are taken into account in the subsequent curve fitting. The normalized signal is equal to $[P \cdot R]/[P \cdot R]_0$, the ratio of the effective volume concentration of target–receptor complexes at a finite ligand concentration to the effective volume concentration of the complexes in the absence of ligands.

than that of the target and thus remain constant during the assay.^{23–25} For solid-supported assays such as microarrays in a microplate, this is not always the case. We thus need to find an appropriate equation for IC_{50} as a function of initial protein concentration ($[P]_0$), initial receptor concentration ($[R]_0$), and equilibrium dissociation constants for target–receptor reaction (K_d) and target–ligand reaction (K_i). One of the goals of measuring IC_{50} is to determine K_i .

For a microarray-in-microplate dose–response assay, receptors are immobilized on the glass surface of the well bottom. The *effective volume concentration* $[R]$ of unoccupied receptors equals the product of the total area (A) covered by printed receptor spots and the surface density (N_s) of *unoccupied* receptors divided by the volume (V) of the aqueous solution in the well, i.e., $[R] = (A/V)N_s$. Both N_s and $[R]$ diminish during the assay. As shown in details in the Appendix, the maximum value of $[R]$ is in the range of 10 pM. Since the initial target concentration $[P]_0 = 100$ nM is much larger than $[R]$, the Cheng–Prusoff equation is not applicable here. Furthermore, the total ligand concentration $[I]_0$ varies from 0.3 nM to 100 μ M and therefore $[I]$ does not necessarily remain constant

either. From the Appendix, the *effective volume concentration* of target–receptor complexes at equilibrium is given by

$$[P \cdot R] = \left(\frac{[P]}{K_d + [P]} \right) [R]_0 \quad (1)$$

In the absence of ligands, the *initial effective volume concentration* of target–receptor complexes is given by

$$[P \cdot R]_0 = \left(\frac{[P]_0}{K_d + [P]_0} \right) [R]_0 \quad (2)$$

The total ligand concentration $[I]_0 \equiv IC_{50}$ at which $[P \cdot R]$ is reduced from $[P \cdot R]_0$ by 50% is given by

$$IC_{50} = \frac{(1 + K_i/K_d)([P]_0)^2 + (K_d + 3K_i)[P]_0 + 2K_dK_i}{2K_d + [P]_0} \quad (3)$$

In our study, $[P]_0 (= 100$ nM) is by choice much larger than K_d (between 0.01 and 1 nM), and as a result eq 3 is simplified to

$$\text{IC50} \cong [\text{P}]_0 \left(1 + \frac{K_i}{K_d} \right) \quad (4)$$

The free ligand concentration $[\text{I}]_{50}$ is given by

$$[\text{I}]_{50} \cong \text{IC50} - [\text{P}]_0 = \frac{[\text{P}]_0 K_i}{K_d} \quad (5)$$

Equation 5 is the same as the Cheng–Prusoff equation for competitive inhibition in the limit that $[\text{P}]_0 \gg K_d$, as one should expect.²⁴

Extraction of Equilibrium Dissociation Constant K_i for Solution-Phase Target–Ligand Reactions. K_i for reactions of the 64 ligands (peptides) with corresponding targets (rabbit monoclonal antibodies raised against the peptides) *in solution* had never been measured before. In separate experiments we measured K_d for reactions of these same but *immobilized* ligands with the antibody targets. One may use eq 4 and values of $[\text{P}]_0$, K_d , and IC50 to extract K_i for target–ligand reactions *in solution*. In our case, we fit the data in Figure 4 to eq A7b using K_i as the fitting parameter. The results are listed in Table 1, along with K_d and IC50 (obtained from eq 4 when $K_d \ll 100$ nM, or eq A10 when $K_d > 100$ nM). For eight ligands, errors in K_i from curve fitting are so large that they render values of K_i unreliable. As a result we do not have K_i for these eight ligands in Table 1, although IC50 can still be determined from the data (curves for these ligands serve as a guide-to-eye only). K_i ranges from 15 pM to 190 nM with the median at 3 nM. On average K_i is significantly larger than K_d (the equilibrium dissociation constant of the same reaction but obtained with the ligands immobilized on a solid surface), by a median factor of 25. One plausible explanation is that the complex formed by the target and an immobilized peptide is further stabilized by nonspecific attraction of other parts of the target to the peptide-covered surface. In this case we expect $K_i > K_d$. Another feasible explanation is that free peptides *in solution* exist as a collection of conformational isomers that transform to one another on a time scale of 10^{-9} s.²⁶ As a result a target needs many collisions with peptides in order to encounter the right isomer to form a complex. For this entropic reason more prevalent for peptides, the association rate constant k_{on} of a target with a peptide in solution can be quite small, well-known to the community of peptide-based drug discovery. When a peptide is immobilized to a solid surface, the number of conformational isomers is reduced. As a result, it takes a target much fewer encounters with immobilized peptides to form a complex and we expect a much larger association rate constant k_{on} and in turn smaller K_d ($= k_{\text{off}}/k_{\text{on}}$). This second explanation seems in contradiction to what one may expect of a diffusion-controlled reaction with $k_{\text{on,diffusion}} = 4\pi(D_T + D_L)(r_T + r_L)(N_A/1000)$, where D_T and D_L in $\text{cm}^2/\text{s}^{-1}$ are diffusion coefficients of the target and the ligand in solution, r_T and r_L in cm are *effective* radii of the target and the ligand, and N_A is the Avogadro constant.²⁷ Since $D_T \sim 5 \times 10^{-7}$ $\text{cm}^2 \text{ s}^{-1}$ and $r_T \sim 5 \times 10^{-7}$ cm for a full-size rabbit IgG molecule, the diffusion-controlled association rate with immobilized ligands is expected to be $k_{\text{on,diffusion}} \sim 2 \times 10^9 \text{ M}^{-1} \text{ s}^{-1}$. This is much larger than k_{on} for binding reaction of IgG with immobilized peptides (2×10^4 to $1 \times 10^6 \text{ M}^{-1} \text{ s}^{-1}$) reported by Landry et al.,²⁸ indicating that the reaction of IgG with immobilized peptides is not diffusion-controlled. We should note that $k_{\text{on,diffusion}}$ is valid when both the target and the ligand are spherical molecules and isotropically reactive. The large disparity between $k_{\text{on,diffusion}}$ and k_{on} for reactions of rabbit

IgG molecules with immobilized peptides is most likely due to two factors. The first is that IgG and peptides are not isotropically reactive. As a result the collision of an IgG molecule with a peptide leads to formation of a complex only when the IgG molecule is properly oriented toward the peptide. Such collisions are a very small fraction of all IgG–peptide collisions. The second factor is that an immobilized peptide still has multiple conformational isomers and only one isomer can form a stable complex with an IgG molecule.

Further Remarks on the Microarray-in-Microplate Platform for Dose–Response Measurement. The present paper describes a proof-of-principle study in which the “ligand” and “receptor” are chemically identical (both 15-aa peptides) except that one is immobilized as “receptor” and the other is in solution as “ligand”. In drug discovery applications, one would immobilize the receptor as microarrays in a microplate. K_d for reaction of a target with the immobilized receptor can be determined separately.²⁸ K_i and IC50 can then be determined by incubating the receptor microarrays in the microplate in solutions of the target and ligands as illustrated in this work.

In addition to the fact that this platform indeed supports high-throughput dose–response measurements when detected by a scanning optical sensor with a large FOV, the capability of detecting surface densities of target–receptor complexes *in real time* ensures that the equilibrium is reached before the data for dose–response curves are acquired. This is not feasible with fluorescence-based plate readers that involve reactions of labeled primary or labeled secondary antibodies with captured targets that may have partly or mostly dissociated from receptors during washing steps.²⁹ Since sequentially added buffers and solutions are not removed from the wells, this platform is readily integrated with commercial liquid handling systems for automation. As for throughputs, one typically performs one competitive assay in a well (instead of two in our present study) and acquires 32 dose–response curves with 12 concentration points. It is feasible to extend the platform to a 1536-well glass-bottomed plate such that 128 dose–response curves can be acquired in one experiment. Such throughput will match the throughput of the microarray-based ligand discovery platform.¹⁰

■ APPENDIX: IC50 FOR MICROARRAY-IN-MICROPLATE INHIBITION ASSAY

Basic Consideration and Definition

We consider a well of a microplate that contains a solution of free protein targets with concentration $[\text{P}]$, free inhibitors with concentration $[\text{I}]$, and “free” surface-immobilized receptors with effective concentration $[\text{R}]$. The total volume of the solution is V . Let A be the surface area covered by immobilized receptors and N_s the surface density of “free” immobilized receptors. We have $[\text{R}] = (A/V)N_s$. In addition, the well also contains protein–receptor complexes with concentration $[\text{P}\cdot\text{R}]$ and protein–inhibitor complexes with concentration $[\text{P}\cdot\text{I}]$. A label-free optical sensor detects the surface density of protein–receptor complexes, and the latter equals $[\text{P}\cdot\text{R}]$ multiplied by (V/A) .

Let $[\text{P}]_0$ be the total protein target concentration, $[\text{I}]_0$ the total inhibitor concentration, $[\text{R}]_0 = (A/V)N_{s0}$ the total receptor concentration, K_i the affinity constant (equilibrium dissociation constant) of solution-phase protein–inhibitor reaction, and K_d the affinity constant of protein targets with immobilized receptors. In equilibrium, we have

$$K_d = \frac{[P][R]}{[P \cdot R]} \quad (\text{A1})$$

$$K_i = \frac{[P][I]}{[P \cdot I]} \quad (\text{A2})$$

From the law of mass conservation, we further have

$$[P]_0 = [P] + [P \cdot I] + [P \cdot R] \quad (\text{A3a})$$

$$[I]_0 = [I] + [P \cdot I] \quad (\text{A4a})$$

$$[R]_0 = [R] + [P \cdot R] \quad (\text{A5a})$$

We now justify a simplifying assumption: $[P]_0 = 100 \text{ nM} \gg [R]_0$ so that eqs A3a–A5a are reduced to

$$[P]_0 \cong [P] + [P \cdot I] \quad (\text{A3b})$$

$$[I]_0 = [I] + [P \cdot I] \quad (\text{A4b})$$

$$[R]_0 = [R] + [P \cdot R] \quad (\text{A5b})$$

Typical surface densities of receptors on a flat solid surface are $N_{s0} \sim 10^{-12} \text{ mol/cm}^2$. The nominal area of a receptor microarray spot is $A_1 = 10^{-4} \text{ cm}^2$. Assume that there are 10 replicates of receptor spots in a well, the total area covered by 10 receptor spots is $A = 10A_1 = 10^{-5} \text{ cm}^2$. For a volume of $V = 10^{-4} \text{ L}$, the total receptor concentration is $[R]_0 \sim AN_{s0}/V = 10^{-11} \text{ M}$. As a result $[P]_0 \gg [R]_0$. This means that protein–receptor reactions have negligible effect on $[P]$.

Dose–Response and IC50

In the absence of inhibitors, the concentration of protein–receptor complexes is arrived at from eqs A1, A3b, and A5b:

$$[P \cdot R]_0 = [R]_0 \frac{[P]_0}{[P]_0 + K_d} \quad (\text{A6})$$

In the presence of inhibitors at a total concentration $[I]_0$, the free protein concentration is reduced to $[P] = [P]_0 - [P \cdot I]$ by protein–inhibitor reactions in solution. This decreases the concentration of protein–receptor complexes to

$$[P \cdot R] = [R]_0 \frac{[P]}{[P] + K_d} \quad (\text{A7a})$$

Using eqs A1–A5, we can express $[P \cdot R]$ as a function of $[P]_0$, $[I]_0$, $[R]_0$, K_d , and K_i as

$$[P \cdot R] = [R]_0 \frac{[P]_0 - [I]_0 - K_i + \sqrt{([P]_0 - [I]_0 - K_i)^2 + 4[P]_0 K_i}}{[P]_0 - [I]_0 - K_i + \sqrt{([P]_0 - [I]_0 - K_i)^2 + 4[P]_0 K_i} + 2K_d} \quad (\text{A7b})$$

We define the total inhibitor concentration $[I]_0$ that reduces $[P \cdot R]$ to one-half of $[P \cdot R]_0$ as IC50. Let $[P]_{50}$ be the free protein target concentration that makes $[P \cdot R]$ to one-half of $[P \cdot R]_0$. From eq A7, we have

$$[P]_{50} = \frac{[P]_0 K_d}{[P]_0 + 2K_d} \quad (\text{A8})$$

From eqs A2, A3b, and A4b, we find the total inhibitor concentration $[I]_0$ as a function of the expected free protein target concentration $[P]$, $[P]_0$, K_d , and K_i as follows:

$$[I]_0 = ([P] + K_i) \left(\frac{[P]_0 - [P]}{[P]} \right) \quad (\text{A9})$$

Combining eqs A8 and A9, we arrive at the formula for $[I]_0 = \text{IC50}$:

$$\text{IC50} = \frac{(1 + K_i/K_d)([P]_0)^2 + (K_d + 3K_i)[P]_0 + 2K_d K_i}{2K_d + [P]_0} \quad (\text{A10})$$

Equation A10 is the same as eq 3 in the main text. Under the condition that $[P]_0 \gg K_d$ so that eq A6 is simplified to $[P \cdot R]_0 = [R]_0$, eq A8 to $[P]_{50} = K_d$, eq A10 is further reduced to

$$\text{IC50} \cong [P]_0 \left(1 + \frac{K_i}{K_d} \right) \quad (\text{A11})$$

It is the same as eq 4 in the main text. To arrive at eq A11, we rewrite eq A10 as

$$\begin{aligned} \text{IC50} &\approx [(1 + K_i/K_d)([P]_0)^2 + (K_d + 3K_i)[P]_0 + 2K_d K_i] \left[1 - \frac{2K_d}{[P]_0} \right] \frac{1}{[P]_0} \\ &= [(P]_0)^2 + [P]_0 K_i ([P]_0 / K_d) - [P]_0 K_d + [P]_0 K_i - 4K_d K_i \\ &\quad - 4K_d K_i (K_d / [P]_0) - 2K_d K_d] \frac{1}{[P]_0} \end{aligned}$$

The seventh term in the bracket is of the order of $(K_d/[P]_0)^2$ and thus dropped. The sixth term is much smaller than the fifth term and dropped. The fifth term is much smaller than the fourth term and dropped. The fourth term is much smaller than the second term and dropped. The third term is small or comparable to the fourth term and thus dropped as well. We have eq A11.

AUTHOR INFORMATION

Corresponding Author

*E-mail: xdzhu@physics.ucdavis.edu.

Notes

The authors declare no competing financial interest.

ACKNOWLEDGMENTS

This work was supported by NIH under R01-HG003827 and R01-HD065122 and by the University of California under UC Discovery Grant No. bio09-156225.

REFERENCES

- (1) Schreiber, S. L. *Nat. Chem. Biol.* **2005**, *1*, 64–66.
- (2) Stockwell, B. R. *Nature* **2004**, *432*, 846–854.
- (3) Gurard-Levin, Z. A.; Scholle, M. D.; Eisenberg, A. H.; Mrksich, M. *ACS Comb. Sci.* **2011**, *13*, 347–350.
- (4) Noah, J. W. *Int. J. High Throughput Screening* **2010**, *1*, 141–149.
- (5) Zang, R.; Li, D.; Tang, I.-C.; Wang, J. F.; Yang, S.-T. *Int. J. Biotechnol. Wellness Ind.* **2012**, *1*, 31–51.
- (6) Szymanski, P.; Markowicz, M.; Mikiciuk-Olasik, E. *Int. J. Mol. Sci.* **2012**, *13*, 427–452.
- (7) Bradner, J. E.; McPherson, O. M.; Mazitschek, R.; Barnes-Seeman, D.; Shen, J. P.; Dhaliwal, J.; Stevenson, K. E.; Duffner, J. L.; Park, S. B.; Neuberger, D. S.; Nghiem, P.; Schreiber, S. L.; Koehler, A. N. *Chem. Biol.* **2006**, *13*, 493–504.
- (8) Duffner, J. L.; Clemons, P. A.; Koehler, A. N. *Curr. Opin. Chem. Biol.* **2007**, *11*, 74–82.
- (9) Hong, J. A.; Neel, D. V.; Wassaf, D.; Caballero, F.; Koehler, A. N. *Curr. Opin. Chem. Biol.* **2014**, *18*, 21–28.

- (10) Landry, J. P.; Fei, Y.; Zhu, X.; Ke, Y.; Yu, G.; Lee, P. *Assay Drug Dev. Technol.* **2013**, *11*, 326–332.
- (11) MacBeath, G.; Koehler, A. N.; Schreiber, S. L. *J. Am. Chem. Soc.* **1999**, *121*, 7967–7968.
- (12) Tolliday, N.; Clemons, P. A.; Ferraiolo, P.; Koehler, A. N.; Lewis, T. A.; Li, X.; Schreiber, S. L.; Gerhard, D. S.; Eliasof, S. *Cancer Res.* **2006**, *66*, 8935–8942.
- (13) Uttamchandani, M.; Walsh, D. P.; Yao, S. Q.; Chang, Y. T. *Curr. Opin. Chem. Biol.* **2005**, *9*, 4–13.
- (14) Lam, K. S. *Anti-Cancer Drug Des.* **1997**, *12*, 145–167.
- (15) Lam, K. S.; Liu, R.; Miyamoto, S.; Lehman, A. L.; Tuscano, J. M. *Acc. Chem. Res.* **2003**, *36*, 370–377.
- (16) Lam, K. S.; Salmon, S. E.; Hersh, E. M.; Hruby, V. J.; Kazmierski, W. M.; Knapp, R. J. *Nature* **1991**, *354*, 82–84.
- (17) Landry, J. P.; Fei, Y.; Zhu, X. *Assay Drug Dev. Technol.* **2011**, *10*, 250–259.
- (18) Landry, J. P.; Fei, Y.; Zhu, X. D. *Int. Drug Discovery*, **2011**, Dec, 8–13.
- (19) Landry, J. P.; Proudian, A. P.; Malovichko, G.; Zhu, X. D. *Proc. SPIE* **2013**, 8587, 1V-1–1V-11.
- (20) Fei, Y. Y.; Landry, J. P.; Sun, Y. S.; Zhu, X. D.; Luo, J. T.; Wang, X. B.; Lam, K. S. *Rev. Sci. Instrum.* **2008**, *79*, 013708-1–013708-7.
- (21) Zhu, X. D.; Landry, J. P.; Sun, Y. S.; Gregg, J. P.; Lam, K. S.; Guo, X. W. *Appl. Opt.* **2007**, *46*, 1890–1895.
- (22) Landry, J. P.; Sun, Y. S.; Guo, X. W.; Zhu, X. D. *Appl. Opt.* **2008**, *47*, 3275–3288.
- (23) Briggs, G. E.; Haldane, J. B. *Biochem. J.* **1925**, *19*, 338–339.
- (24) Cheng, Y.; Prusoff, W. H. *Biochem. Pharmacol.* **1973**, *22*, 3099–3108.
- (25) Michaelis, L.; Menten, M. L. *Biochem. Z.* **1913**, *49*, 333–369.
- (26) Verdine, G. L.; Walensky, L. D. *Clin. Cancer Res.* **2007**, *13*, 7264–7270.
- (27) Alberty, R. A.; Hammes, G. G. *J. Phys. Chem.* **1958**, *62*, 154–159.
- (28) Landry, J. P.; Ke, Y.; Yu, G. L.; Zhu, X. D. *J. Immunol. Methods* **2015**, *417*, 86–96.
- (29) Bradner, J. E.; McPherson, O. M.; Koehler, A. N. *Nat. Protoc.* **2006**, *1*, 2344–2352.